First measurement of the absorption of $^3\overline{\mathrm{He}}$ and $\bar{\mathrm{t}}$ nuclei in matter and impact on $^3\overline{\mathrm{He}}$ propagation in the galaxy

Stephan Koenigstorfer

XX.XX.2022

Abstract

Abstract goes here at the end

Contents

1 Introduction

1.1 The goal of this work

1.2 The standard model of particle physics

1.3 Matter and antimatter in the universe

1.3.1 Origin of hadronic matter

1.3.2 A matter dominated universe: antimatter-matter asymmetry

1.4 Antimatter-matter annihilations

1.4.1 Antiproton-matter annihilations on different materials

1.4.2 Antinuclei-matter annihilations: the Glauber model and geometric scaling

1.4.3 The effect of the coulomb interaction on antinuclei-matter annihilations

1.5 Antinuclei in the cosmos

1.5.1 Why producing antinuclei is so difficult: production mechanisms of antinuclei

$$B_N = E_A \frac{d^3 N_A}{dp_A^3} \left[\left(E_{p,n} \frac{d^3 N_{p,n}}{dp_{p,n}^3} \right)^A |_{\vec{p}_p = \vec{p}_n = \vec{p}_A/A} \right]^{-1} \quad (1)$$

1.5.2 Why to we care: antinuclei as a golden channel for new physics

1.5.3 What affects antinuclei in cosmic rays: production, propagation and annihilation

1.5.4 How can antinuclei in the cosmos be detected: AMS, GAPS, cubesats

1.6 Antinuclei on earth

1.6.1 Production at accelerators

1.6.2 Annihilation at accelerators

1.6.3 Previous status of knowledge on antinuclei annihilation

1.7 Dark matter and its connection to antinuclei

1.7.1 The evidence for dark matter

1.7.2 WIMP dark matter and the WIMP miracle

1.7.3 Dark matter annihilations into antinuclei

1.7.4 Majorana vs. Dirac dark matter

Since the properties of dark matter are not know beyond its gravitational pull, it is also not known if dark matter is its own anti-particle.

1.7.5 Thermal self-annihilation cross section in the early universe

1.7.6 The ditribution of dark matter within our galaxy

1.7.7 The search for dark matter: the link between WIMP dark matter and antinuclei

Figure 1: Ratio of antiprotons to protons produced at mid-rapidity as a function of beam rapidity. At ALICE energies the value approaches unity, demonstrating that at such high energies antimatter and matter are produced in almost equal amounts.

2 Experimental data

2.1 ALICE

2.1.1 Overview

- Trigger System
- ITS
- TPC
- TOF

2.1.2 Basics of ALICE data structure

2.1.3 Collision system and event cuts

2.1.4 Reconstruction of raw (anti)nuclei

2.1.5 Raw $^3\overline{\mathrm{He}}/^3\mathrm{He}$ ratio

2.1.6 Raw antitriton-to-triton ratio

2.1.7 Correction for secondaries from material spallation

2.1.8 Annihilations within the detector

2.2 Extracting the inelastic cross section from the antimatter to matter ratio

2.2.1 Comparison of ratios with Monte Carlo simulations

In order to fairly compare the Monte Carlo simulations to the produced data, it is vital to account for the baryochemical potential[1] at such high energies. The relevant ratio of antiprotons to protons is shown in figure **??**. Based on the same arguments as the formula for the coalescence parameter 1, the effect on the ratio of antinuclei will be the same as to the antiproton-to-proton ratio taken to the exponent of the mass number of the antinucleus.

[1] In other words: how much more antimatter particles we have for each matter particle. Given that we collide purely matter particles, there is a penalty for producing antimatter, even though at such high energies it is vanishingly small.

2.2.2 Ratios as a function of the inelastic cross section

2.2.3 Non-linear error propagation

2.2.4 Accounting for energy losses between the primary vertex and the point of annihilation

2.2.5 Uncertainty coming from the material budget

2.2.6 Evaluating the average material for antinuclei annihilations in the ALICE detector

2.2.7 Independence of collision system

The antimatter-to-matter ratio method's dependence on collision system has been investigated by redoing the analysis performed in pPb collisions in [**?**] for high multiplicity pp collisions. The dependence on the collision system is due to the multiplicity differences, and the resulting difference in the baryochemical potential as discussed in section 2.2.1. By taking the antiproton-to-proton ratio for the different collision systems and comparing them, the predicted difference between the antideuteron-to-deuteron ratio was obtained. The results are shown in figure **??**, which show that the differences between collisions systems are consistent with the expected deviation. This independence of the collision system is expected, since the inelastic cross section is completely independent on the collision system. This becomes especially self-evident when considering that the annihilations do not occur in the initial collisions, but rather as the antiparticles travel through the detector material.

Figure 2: Ratio of the antiproton-to-proton ratios (left) and antideuteron-to-deuteron ratios (right) obtained in high multiplicity pp collisions and in pPb collisions, compared to the expected difference from the different baryochemical potentials (dashed red line).

3 Measurement of the $^3\overline{\mathrm{He}}$ inelastic cross section

3.1 Physics motivation and overview of the analysis method

3.2 Analysis techniques

3.2.1 Antimatter-to-matter ratio method

3.2.2 TOF-TPC matching method

3.3 Secondary correction

3.4 Results

4 Measurement of the antitriton inelastic cross section

4.1 Physics motivation and overview of the analysis method

4.2 Analysis technique

4.2.1 Antimatter-to-matter ratio method

4.2.2 TOF-TPC matching method

4.3 Feasibility of the momentum range

4.4 Secondary correction

4.5 Results

5 Antinuclei in the cosmos

The goal of this section is to discuss possible exotic sources of antinuclei in our galaxy: i) WIMP dark matter and ii) extragalactic WIMP dark matter. These are compared to antinuclei produced in high energy cosmic ray collisions, which is a process we know to occur. In order to study these sources and their effect on a signal near earth, we employ the GALPROP framework. This framework propagates particles through our galaxy, simulating various effects such as diffusion, convection and also includes annihilation effect. The resulting fluxes near earth are then presented for both antideuterons and $^3\overline{\mathrm{He}}$, for different dark matter masses and profiles. Finally, current and planned experiments for detecting antinuclei in cosmic rays are discussed.

5.1 Sources of antinuclei in the cosmos

Antinuclei are some of the rarest particles in our galaxy, since very few abundantly occurring processes will produce them in any non-negligible amount[]. A large amount of the light matter nulcei (up to Lithium) were produced during Big Bang Nucleosynthesis (BBN)[], while all heavier nuclei are produced during stellar nucleosynthesis[]. However, due to the asymmetry of matter and antimatter in our galaxy, neither of these methods is thought to be a dominant source for antinuclei. Antimatter produced during BBN is likely to have annihilated propagating through the galaxy from the Big Bang until today, and since we have no evidence that anti-stars exist[], it is unlikely that antinuclei could be produced through stellar nucleisynthesis.
We therefore have to look to other processes which could produce antinuclei. Due to baryon number conservation, all such processes are likely to produce at least an equal amount of light nuclei as well, however, since nuclei are far more abundant than antinuclei, these processes will only contribute a neglibigle amount to the total antinuclei flux in our galaxy. This extremely high expected signal to background ratio is the reason why antinuclei are considered such a promising probe into new physics.

5.1.1 High energy cosmic ray collisions

5.1.2 Weakly interacting massive particles (WIMPs) - dark matter

Some WIMP dark matter theories predict that WIMP annihilations can produce a significant amount of antinuclei []. This can be understood simply from the available energy in such a process. A cold dark matter particle pair annihilating would have $\sqrt{s}= 2\mathrm{m}_\chi$. The net baryon number would be 0 in such a process, resulting in no further penalty for the production of multiple antinucleons. Per definition, WIMPs would interact only weakly, and thus their initial annihilation channel would go through a weak channel. Since the weak bosons couple to all other standard model particles, this enables a decay into standard model particles.

The spectrum and yield of antinuclei produced in these annihilations has to be estimated based on known standard model processes. To this end, Monte Carlo event generators are employed[], in which the initial state is the first state of standard model particles (such as W^+W^- or $b\bar{b}$) which is assumed to occur in the annihilation process, with a COM energy equal to twice the dark matter mass m_χ Since event generators do not produce (anti)nuclei – but only the individual nucleons – the (anti)nuclei yields and spectra have to be calculated using the coalescence model[2].

The WIMP dark matter is assumed to be cold. As such, the COM frame is assumed to be the same as the galactic frame, and no boost from the initial velocities are necessary. This is convenient, since one can therefore simply take the spectrum of produced antinuclei per dark matter annihilation – which is obtained from applying a coalescence afterburner to the output of a Monte Carlo event generator – and multiply it by the local annihilation rate of dark matter. Thus, one can write the source term $q(\vec{r}, E)$ for WIMP dark matter as is written in equation 2.

$$q(\vec{r}, E) = \frac{1}{2}\left(\frac{\rho_\chi(\vec{r})}{m_\chi}\right)^2 < \sigma v > \frac{dN}{dE} \tag{2}$$

where the factor $1/2$ comes from symmetry considerations for majorana dark matter[3], the term $\left(\frac{\rho_\chi(\vec{r})}{m_\chi}\right)^2$ is the square of the number density of the WIMP dark matter, which is then multiplied by the velocity averaged dark matter annihilation cross section $< \sigma v >$, giving the rate of dark matter annihilations for a given point in space. The final term of equation 2 is the spectrum of produced antinuclei normalised to a single dark matter annihilation.

The dark matter density profile $\rho_\chi(\vec{r})$ affects both the total amount of antinuclei produced as well as their initial distribution. This parameter can be constrained from measurements of the milky way's rotational curve, similarly to how it is done for other galaxies. However, measuring the rotation curve of the Milky Way involves extra challenges, given that we are measuring from within. For other galaxies, the rotational velocities of the stars can be measured from their red/blue shift, and their position in respect to the galactic center is easily estimated by their angular displacement. For stars in our own galaxy, we cannot purely rely on the angular position of a star in the sky in order find the displacement of the star in respect to the galactic center, as the star could be anywhere in the galactic plane within this line of sight. This is illustrated on the right of figure **??**. It is therefore necessary to determine not only position in the sky, but also the distance to the star in question. Similarly, the rotational velocity

[2]See Appendix 7.2 for an explaination of why the statistical hadronization model cannot be used to calculate (anti)nuclei yields from dark matter annihilations

[3]See section 1.7.4 for a discussion on the difference between Majorana and Dirac dark matter.

of the stars has to take into account that we can only measure the velocity component normal to our position. The consequence of these difficulties is that the uncertainty on both the position and rotational velocity of stars increases the further away from us the star is. Such a measurement of our galaxy's rotation curve has been reported in [], and is shown in figure **??**.

Figure 3: Left: This shows the method for measuring the rotation curves for galaxies other than the milky way. The displacement from the center of the galaxy is measured by measuring angular displacement. The rotational velocity can be extracted by measuring the red/blue shift of the star[]. Right: This diagram shows the method for measuring the rotational velocity and position of stars within our galaxy.

Figure 4: Rotation curve of stars in the Milky Way, as a function of distance from the galactic center.

In order to fit such rotation curves, our galaxy is conventionally split into individual parts, each of which can be assumed to have a simpler shape. The usual breakdown of these parts is shown in table 5.1.2, and further details can be found in [**?**]. The gravitational potentials of these parts can then be summed up linearly, and the rotational velocities caused by each such potential can be added in quadrature. In order to fit the contribution from dark matter, the shape of the dark matter distribution has to be chosen a priori, such that the exact parameters and normalization can then be obtained from the fit. This is an important point, since the total normalization of the dark matter profile is not well constrained. Rather, the relatively well constrained rotation curve in the proximity of the solar system results in the fact that the local dark matter density $\rho_\chi(\vec{r} = r_\odot) := \rho_\chi^\odot$ is much better constrained than the total normalization of the dark matter profile. Thus, the different dark matter profiles are constrained to their value at $r_\odot = 8.5$kpc.

Table 1: Individual axissymmetric parts of the Mikly Way used for fitting rotation curves. The distinction is made in order to simplify the fit, rather than a hard distinction within the actual galaxy. Non-axissymmetric components are neglected for rotation curves, based on the assumption that any effects would cancel out when averaged over the full rotation.

Part	Shape	Extent	Total Mass
Central black hole	Point mass	¡¡0.1pc	xx M⊙
Buldge(s)	Spherical exponential	XXkpc	xx M⊙
Flat disk	Constant flat disk	XXkpc	xx M⊙
Dark matter halo	vaires	XXkpc	xx M⊙

There are several profiles on the market, which achieve similar goodness-of-fit when fit to account for the dark matter component in the rotation curve[], while also achieving the required normalisation at $r_{\odot}$. The ones used in this work are the Navarro-Frenk-White(NFW) profile[], shown in equation 3,

$$\rho_{\chi}^{NFW}(\vec{r}) = \frac{\rho_0}{(r/r_s)[1+(r/r_s)]^2} \tag{3}$$

with scale radius r_s =24.42kpc. The Einasto profile[], shown in equation 4,

$$\rho_{\chi}^{Einasto}(\vec{r}) = \rho_0 exp\left\{-\frac{2}{\alpha}\left[\left(\frac{r}{r_s}^{\alpha} - 1\right)\right]\right\} \tag{4}$$

with α=0.17 and r_s=28.44kpc, and the much shallower isothermal profile [] and the isothermal profile, shown in equation 5

$$\rho_{\chi}^{isothermal}(\vec{r}) = \frac{\rho_0}{r^2 + r_s^2} \tag{5}$$

with r_s=4.38kpc. The profiles are plotted in figure 5, using best fit values taken from [**?**]. It can be seen that the isothermal profile has a very shallow rise towards the galactic center, while the Einasto profile rises very steeply. The NFW profile lies between the two, and is often used preferentially []. These three profiles cover most of the available parameter space for the dark matter profile.

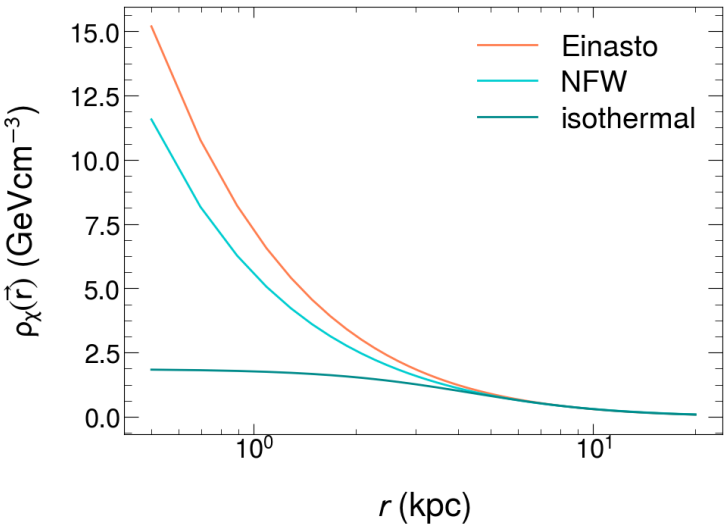

Figure 5: Dark matter density profiles used in this work, as a function of the distance to the galactic centre. The best fit values for each profile are taken from **??**

It is important to ask why the stark differences towards the center of the galaxy play such a reduced role that all three of these profiles are able to fit the data, and if such differences would therefore make any interpretation of an antinuclei flux from dark matter impossible. The answer to the first part of the question is twofold. Firstly, it is very challenging to measure the rotation curve of our own galaxy with high precision at positions far from the solar system. Secondly, the gravitational effect of the dark matter halo contributed mainly at larger distances from the galactic center, where the presence of extra mass at the centre of our galaxy (from a steeper profile) is not as strongly felt. The second question also has a fortunate answer: the effect of different profiles on the local fluxes of antinuclei from a potential dark matter source is rather small, as is discussed in section 5.6.2.

The dark matter mass is a free parameter, with possible dark matter masses ranging from very light dark matter[4] in the eV range all the way to the WIMP dark matter discussed in this work, with plausible mass ranges from 10s of GeV to the TeV range. As discussed in section 1.7.2, the appeal of WIMP dark matter is that the expected weak cross section of such a particle in the very early universe would yield a population today of the same magnitude as we observe. It would also explain the lack of evidence for the production of dark matter at accelerators, since we might at this point not yet have reached the energies required to even produce these particles[5]. Since the exact nature of dark matter remains a mystery, any mass within this WIMP range which is not excluded by other measurements can be assumed. The chosen mass has a direct effect on all three remaining terms of equation 2: i) $\frac{1}{m_\chi^2}$, ii) $< \sigma v >$ and iii) $\frac{dN_{\bar{p},\bar{d},^3\overline{He}}}{dE}$. The effect on i) is trivial, and reduces the overall normalization of the antinuclei source term for higher m_χ The mass' effect on iii) is based on the amount of energy available for the production of (anti)nuclei, as well as for their kinetic energy. For higher masses, the antinuclei yields increase non-trivially, but less fast then the inverse square reduction from the first term. Additionally, the extra energy available for higher masses translates into a spectrum peaked at higher momenta. The effect on ii) is mostly experimental, since $< \sigma v >$ is constrained from antiproton measurements. Any dark matter annihilation process which can result into antideuterons must of course also produce antiprotons. However, contrary to heavier antinuclei, antiprotons are also copiously produced in other processes, resulting in a significant and well constrained antiproton flux, which has been measured by the AMS collaboration []. Thus, any model we choose must not produce a dark matter component for antiprotons which is incompatible with those measurements. These limits are expressed in terms on $< \sigma v >$ as a function of m_χ This representation is chosen since ρ_χ can be measured independently, and iii) varies much more slowly with $m_\chi$than the other

[4] A popular light dark matter model is the axion dark matter model [].

[5] Additionally, some supersymmetric partners could have exactly these required properties, which would make them suitable dark matter candidates[]. However, the lack of evidence for supersymmetry makes this argument somewhat weaker than it was during the inception of WIMPs []

terms. The limits – which have been extracted by several groups [] and compiled by []– are shown in figure 6. Indicated in the figure is the maximum limit on $< \sigma v >$, as extracted by several research groups, as well as the "thermal value", which is the value expected for a WIMP particle with the current abundance of dark matter in the universe. Also indicated in this figure is the region in which a possible excess of antiprotons was observed, which could hint at a dark matter particle within this mass range of 50-100GeV/c^2. It can be seen from the left hand side of the figure that for low dark matter masses, the limits lie significantly below the thermal value for this cross section. Thus, $m_\chi$affects the constraints on $< \sigma v >$, particularly for low masses. It is also worth noting that these limits have to be extracted for a given dark matter density profile, and thus when exploring the maximum allowed antinuclei flux given the antiproton constraints, the choice of profile is degenerate with the limits on $< \sigma v >$ set by AMS antiproton limits.

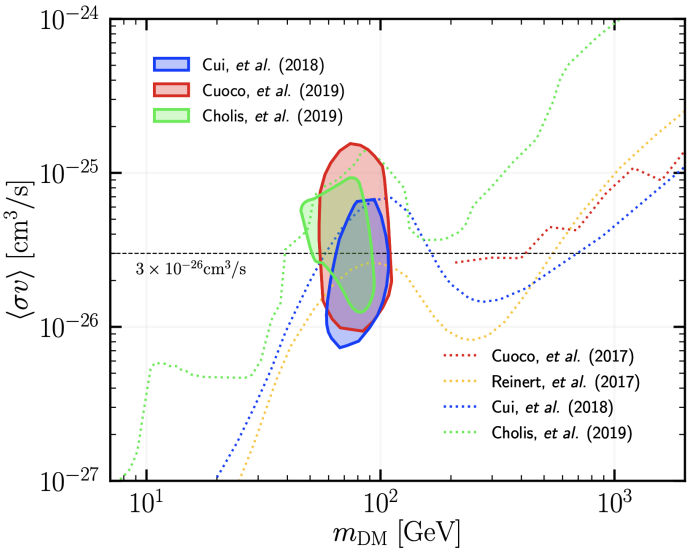

Figure 6: Limits on $< \sigma v >$ based on AMS antiproton data. Figure by [] and reproduced here for easy of access.

To summarise: WIMP dark matter models predict that dark matter can annihilate into antinuclei. The resulting antinuclei source term depends on 4 things: i) the dark matter density profile, ii) the dark matter mass, iii) the dark matter self-annihilation cross-section and iv) the produced spectrum of antinuclei, normalised to dark matter decays. i) is constrained by looking at the rotation curve of our galaxy, ii) is a free parameter, iii) is constrained by antiproton measurements as a function of $m_\chi$and iv) is calculated based on coalescence models, which depend on the total available energy and thus m_χ Thus,

there are a few notable degeneracies between the different terms of this source function. However, current constraints on these parameters are not stringent and leave open a large, reasonable parameter space in which an antinuclei flux from dark matter could be found, affirming antinuclei studies as a great tool for the indirect search for dark matter.

5.1.3 Extragalactic dark matter

Dark matter is not exclusively bound within galaxies, but is also present in larger cosmological structures, such as galaxy groups. However, the profiles commonly used in order to fit the distribution of dark matter within our galaxy only take into account galactic dark matter, which can be inferred from the fact that such profiles go to 0 at large distances from the galactic centre. This is because to first order, the extragalactic component will vary over length scales bigger than our galaxy, so the gravitational potential caused by the extragalactic dark matter will be roughly constant within our galaxy, thus causing no active force which could be measured. However, such an additional flux of dark matter could indeed annihilate within our galaxy, thus providing an additional source for antinuclei. In this section the difference of this source to the galactic WIMP dark matter source will be qualitatively discussed.

In order to determine weather the antinuclei flux caused by extragalactic dark matter follows the same assumptions as the galactic component, it is necessary to examine the differences between galactic and extragalactic dark matter. The first difference would be their velocity. Since the galactic component is bound and the extragalactic is not, the extragalactic component's velocity must exceed the escape velocity of the Milky way, which lies at about 600km/s. This change in velocity may affect 2 terms in equation 2: the self annihilation cross section and the spectrum of produced antinuclei due to the boosted frame in which the collision takes place.
Starting with the change on the self annihilation cross section, this might be due to the momentum dependence of the s-wave and p-wave contributions CHECK DETAILS AND REFERENCE. The s-wave is velocity independent, while the p-wave contribution has a square dependence on the velocity. However, the speeds of 600km/s still only equate to a beta of 0.002, thus the contribution of the s-wave still dominates at these speeds, resulting in no change in regards to galactic dark matter. In a similar fashion it can be shown that the effect of the increased speed on the produced antinuclei spectrum is negligible.

The effect which remains is that of the overall normalisation, which is influenced by the extragalactic component to ρ_χ. This extra component would have little to no effect on the rotation curve of our galaxy, and therefore causes a positive offset in comparison to the purely galactic case. The exact nature of this offset should to first order be roughly constant over our galaxy, however, the interaction of the extragalactic dark matter with our galaxy's gravitational pull would cause an increase in the local extragalactic dark matter density in

comparison to another point within the local group. Thus, the main difference between the extragalactic dark matter and the galactic dark matter is the consideration of where the majority of annihilations would occur. Finally, we can conclude that since the overall normalisation for antinuclei fluxes from dark matter annihilations is constrained by the maximal allowed flux from antiprotons – as discussed in section 5.1.2 – the increase in flux due to an additional extragalactic dark matter component does not significantly impact expectations.

Previous work on the topic expects the extragalactic dark matter component to make up about 12% of the local dark matter abundance close to our solar system[]. From this, it can be estimated that the extragalactic dark matter is responsible for no more than $\approx 20\%$ of the antinuclei flux near earth.

5.2 Constraining the propagation through the galaxy

In the process of propagating thorough our galaxy, particles undergo several different effects. They get produced at various points in both space and time, for example most heavy nuclei are produced in supernovae. As they then propagate from their source towards their eventual detection point near earth, they undergo diffusion effects, as they get mainly elastically scattered by the magnetic fields of the galaxy and individual celestial objects. They are also under the effect of bulk motion via convection effects. Finally, there are various effects which might cause a particle to disappear, mainly inelastic interactions with the interstellar medium, or breakup for unstable particles. All of these processes are characterised by the transport equation [], which is reproduced in equation 6

$$\frac{\partial \psi}{dt} = q(\mathbf{r}, p) + \mathbf{div}(D_{xx}\mathbf{grad}\psi - \mathbf{V}\psi) + \frac{\partial}{\partial p}p^2 D_{pp}\frac{\partial}{\partial p}\frac{\psi}{p^2} - \frac{\partial}{\partial p}\left[\psi\frac{dp}{dt} - \frac{p}{3}(\mathbf{div}\cdot\mathbf{V})\psi\right] - \frac{\psi}{\tau_f} - \frac{\psi}{\tau_r} \tag{6}$$

, where ψ is the time and space dependent flux of a given cosmic ray species, $q(\mathbf{r}, p)$ is the source term as a function of position and momentum, $D_{xx}$and D_{pp} are diffusion and convection parameters, V is the potential felt by the particles CHECK THIS, and τ_f and τ_r are parameters characterising the annihilation and fragmentation rates, respectively. This equation can be solved for a given set of parameters both analytically or numerically. Several tools exits in order to solve this equation, with the most well known being GALPROP[], Dragon [] and XXX. In this work, GALPROP was used, as will be explained in section 5.3.

It is important to note that only the first and final term of equation 6 – i.e. the source and loss terms – depend on the species of particle which is being considered. The other terms, which cover the actual propagation through the galaxy, depend solely on parameters which are common to all particle species. This can be understood as the same magnetic fields and bulk motion affecting all particles. Thus, these parameters can be constrained by fitting abundant cosmic ray species which are sensitive to a particular parameter, in order to

Figure 7: Fluxes of several cosmic ray nuclei, as measured by AMS-02, compared to the predictions of the best-fit values obtained by fitting several key species[]. Reproduced here for clarity.

constrain the propagation for all species. This is particularly important for the propagation of antinuclei, which are extremely rare. These propagation parameters have been investigated and reported by Boscini[] and Cuoco []. The effectiveness of these fits can be seen by comparing predicted spectra of protons, antiprotons and heaver cosmic ray nuclei with the measurements done by AMS-02, which are shown in figure **??**. It can be seen that the predictions work very well for large energies, and there is a smooth response at low energies, which is well understood based on the effects of the heliosphere. This shows that the propagation is well under control.

The effect at low energies is due to the effect of the heliosphere, which is not included in codes such as GALPROP. These codes can only simulate large scale effects, and as such they output the particle fluxes outside of our solar system. Within our solar system, the solar magnetic field will affect incoming charged particles, and this needs to be accounted for. There are tools which treat this in great detail, such as Helmod [], but there are currently no such tools on the market which are able to treat antinuclei. Thus, a simple force field model has been commonly used for this purpose in the literature []. The advantage of this model is its broad applicability, while its disadvantage is mainly a large uncertainty induced for low momentum particles[].

5.3 The Galprop framework

THIS ENTIRE SECTION NEEDS SOME CHECKING TO BE SURE WHAT IM WRITING IS CORRECT! As already discussed in section 5.2, the Galprop framework functions by solving the transport equation (equation 6). It does so by finding a steady state solution, iterating in smaller and smaller timesteps until a stable solution is found. During each timestep, it iterates over a position and momentum grid, the former of which can either be expressed in 2 dimensions (r and z) or 3 (x, y, z). Since we assume axial symmetry, the two are mathematically equivalent, so for the purpose of this work, the 2 dimensional solution was chosen.

Galprop is configured by passing a set of parameters from an external text file. The important parameters are shown in table 2. Of particular note are the Galaxy half height z_h, and the diffusion parameter $D_{SomethinSomethin}$, since the predominant way of constraining these two parameters (the B/C raio? CHECK THIS) is degenerate. The actual parameter which is being fixed is the ratio of the two.

It is important to note that the main parameter which a lot of propagation

Table 2: Parameters for the tuning of Galprop. These are equivalent to the configuration of the galaxy and the propagation parameters in equation 6.

Parameter	Purpose	Best fit value from Boscini	Best Fit value from Cuoco
z_h	Half the height of the galactic disk	4.2kpc	6.2kpc

is the so called grammage, which is the amount of matter of the interstellar medium which particles have to traverse. This is obviously a product of the density of the interstellar medium and the path length of the particles.

Antinuclei are not by default includuded in Galprop, so in order for them to be propagated they had to be inserted into the framework. Fortunately, the framework is capable of handling negative nuclei with antiprotons, therefore the extension was done by providing the mass of the antideuteron/antihelium, their inelastic cross sections on the interstellar medium, and their source functions. Seperate entries were used for the secondary production from high energy cosmic rays and from dark matter annihilations. The inelastic cross section had to be provided on a proton and helium target, which are significantly lighter than the average detector materials probed in the measurements shown in section 3, therefore the results had to be extrapolated to these lighter targets. The exact methods of the extrapolations are explained in section 5.4.

For the source functions,

5.4 Annihilations within our galaxy

The general shape of the antinucleus-proton cross section in Geant4 was modified by the measured deviation from the antinucleus-target cross section reported in sections 3, 4 and in [].

5.5 Results for antideuterons

5.5.1 Results for different dark matter masses

5.5.2 Results for different dark matter profiles

5.6 Results for $^3\overline{\mathrm{He}}$

5.6.1 Results for different dark matter masses

5.6.2 Results for different dark matter profiles

5.7 Experiments to detect antinuclei in the cosmos

5.7.1 Baloon and space bourne experiments

5.7.2 Developing a cubesat for detecting antiprotons

6 Final remarks and outlook

7 Appendix

7.1 Current status of the evidence for and against (but mostly against) the existence of anti-stars

As has been covered plenty already in this thesis, one of the biggest remaining mysteries in physics is the asymmetry between the amount of matter and anti-matter present in our universe. It is thought that up to 95% of luminous matter consists of matter rather than antimatter[]. But how can it be known that another star is not entirely comprised of antimatter, given that the only difference in particles is their electric charge? The answer lies in the fact that even though structures within our galaxy and even universe are filled with only extremely low densities, they are not actually empty. It therefore stands to reason that if there were a region dominated by antimatter (even just a single anti-star, although a larger region seems more likely), such a region would eventually have to end and come in contact with a matter dominated region. In this volume of overlap, antimatter-matter annihilations would occur abundantly, resulting in a significant amount of high energy gamma rays. Such a specific and localized signal should be relatively easy to detect with dedicated gamma ray surveys, such as XXX[] and XXX[]. The lack of any evidence thereof suggests that there are not antimatter dominated regions, and thus no anti-stars.

7.2 Why the statistical hadronization model is not used for calculating (anti)nuclei yields from WIMP dark matter annihilations

7.3 Adding rotational velocities